MecSol2013
International Symposium on Solid Mechanics
April 18-19, 2013
Porto Alegre, Rio Grande do Sul, Brazil

Size effects on nano-indentation considering higher order crystal plasticity

E. Bittencourt
Departamento de Engenharia Civil
Universidade Federal do Rio Grande do Sul
eduardo.bittencourt@ufrgs.br

ABSTRACT

A higher order crystal plasticity formulation, where displacements and crystal slips are independent variables, is proposed here to simulate the behavior of the nano-indentation of single crystals. Higher order boundary conditions are also considered. The effect of geometrically necessary dislocations is taken into account considering an energetic hardening. An artificial viscous effect is introduced in a way that the methodology is able to simulate, in the limit, rate dependent and rate independent constitutive laws. The methodology is implemented within a finite element context. Attention is restricted to two-dimensional cases. Slip system rotations are neglected. Analyses of the indentation considering up to three active slip systems are carried out considering rigid indenters. When higher order terms are taken into account, a size dependent hardness emerges. A comparison with experiments indicates the most appropriate higher order boundary condition for indentation.

Keywords: Dislocation, crystal plasticity, finite element.

1 INTRODUCTION

The consideration of the effects of geometrically necessary dislocations (GNDs) [1, 2] gives rise to a material response that is size dependent, as observed in experiments [3, 4, 5]. Nonlocal crystal plasticity theories that take into account these dislocations have been proposed in the last few years. These theories can be broadly separated in two categories: those that consider higher order boundary conditions [6, 7, 8, 9, 10, 11] and those that do not [12, 13, 14]. The first category of theories will be called here simply as higher order and the second, lower order. While lower order theories are much simpler to implement in an existing conventional plasticity code, in some cases, such as the development of boundary layers [15], these theories fail to reproduce material behavior. On the other side, higher order theories may introduce numerical problems that are not solved completely so far and difficulties to regard boundary conditions. Despite these difficulties, examples of numerical applications in a finite element context can be found in the literature [16, 17, 18, 19, 20], but are in general less disseminated than applications to lower order theories. Besides, in all these cases, applications are restricted to relatively simple boundary conditions and/or less than three active slip systems.

In order to take into account higher order boundary conditions, additional degrees of freedom should be considered. This constraint leads to mixed formulations, which is the focus of the present work. As here the theory of Gurtin [7] is followed, crystal slips are considered independent variables, besides displacements.

Constitutive laws for crystal plasticity can be rate dependent or not. In the case of rate independent plasticity, uniqueness concerns were raised in the past [21, 22], which lead the consideration of material rate sensitivity by Pierce et al. [23], eliminating the problems. Also, rate independent formulations have been recently addressed in alternative ways [24, 25] in order to deal with the uniqueness issue. However, all these studies are based on the classic framework, where displacements are the only independent variable.

In the present work, some numerical difficulties inherent to mixed formulations, including uniqueness and locking issues, are tackled considering multiple slip systems. In particular, the rate independent crystal plasticity presented by Bittencourt et al. [16] is revised. One fundamental change in the formulation presented here is related to elastic points. It is proposed the introduction of an artificial viscous effect for these points, in a way similar to rate dependent formulations. The result is a formulation that, in the limit, can be seen as rate dependent or rate independent depending on the value of the artificial viscosity. In addition, non-trivial applications of the formulation to plain strain wedge indentation are explored.

At first, the mixed crystal plasticity theory proposed by Gurtin [7], where slips are independent variables, is outlined (Section 2). The theory is here restricted to plain strain, rate independent plasticity and slip system rotations are neglected. Dissipative hardening is related to the density of statistically distributed dislocations and kinematic hardening is related to the density of GNDs. The discretization of the theory within a finite element framework is described in Section 3. Application of the theory to solve indentation cases is presented in Section 4. The measured hardness by the simulation is shown and compared with expected results. Different higher order boundary conditions are also discussed. Finally, Section 5 contains the conclusions of this work.

2 CRYSTAL PLASTICITY FORMULATION

The calculations are based on the higher order gradient crystal plasticity theory of Gurtin [7] which is briefly described here. Attention is confined to plane strain. The gradient of the displacement vector, $u_{i,j}$, is written as the sum of an elastic u^e_{ij} and a plastic u^p_{ij} part. The plastic part occurs by crystallographic slip on a set of slip planes. With $s^{(\beta)}_i$ and $m^{(\beta)}_i$ unit vectors specifying the slip direction and the slip plane normal, respectively, for slip on a system β, the plastic part of the displacement gradient is given by

$$u^p_{ij} = \sum_\beta \gamma^{(\beta)} s^{(\beta)}_i m^{(\beta)}_j \tag{1}$$

with $\gamma^{(\beta)}$ the total slip on the system β. Greek superscripts, with no summation convention, are used to label the slip systems. Slip system directions are considered fixed throughout calculations. It is assumed also that plastic strains do not produce volume change and elastic strains are isotropic and infinitesimal.

With body forces neglected, the principle of virtual work can be written as

$$\int_B \left[\sigma_{ij}\delta u_{i,j} + \sum_\beta \left(\pi^{(\beta)} - \tau^{(\beta)}\right)\delta\gamma^{(\beta)} + \sum_\beta \xi^{(\beta)}_i \delta\gamma^{(\beta)}_{,i}\right] dV =$$

$$\int_{\partial B_q} \sum_\beta q^{(\beta)}\delta\gamma^{(\beta)} dA + \int_{\partial B_t} t_i \delta u_i dA. \tag{2}$$

Here, $t_i = \sigma_{ij} n_j$, $q^{(\beta)} = \xi^{(\beta)}_i n_i$ where n_i is the surface normal, ∂B_t is the part of the boundary on

which t_i is prescribed, ∂B_q is the part of the boundary on which $q^{(\beta)}$ is prescribed and

$$\tau^{(\beta)} = P_{ij}^{(\beta)}\sigma_{ij} \quad , \quad P_{ij}^{(\beta)} = \frac{1}{2}\left(s_i^{(\beta)}m_j^{(\beta)} + s_j^{(\beta)}m_i^{(\beta)}\right). \tag{3}$$

The quantities $\pi^{(\beta)}$ and $\xi_i^{(\beta)}$ are specified through constitutive relations. The macro boundary conditions are that at each point on the boundary either t_i or u_i is prescribed and the corresponding micro boundary conditions are that either $q^{(\beta)}$ or $\gamma^{(\beta)}$ is prescribed.

Since Eq. (2) holds for independent variations in δu_i and $\delta\gamma^{(\beta)}$, the principle of virtual work can be separated in two parts as

$$\int_B \sigma_{ij}\delta u_{i,j}dV = \int_{\partial B_t} t_i\delta u_i dA \tag{4}$$

and

$$\int_B \left[\sum_\beta \left(\pi^{(\beta)} - \tau^{(\beta)}\right)\delta\gamma^{(\beta)} + \sum_\beta \xi_i^{(\beta)}\delta\gamma_{,i}^{(\beta)}\right]dV = \int_{\partial B_q}\sum_\beta q^{(\beta)}\delta\gamma^{(\beta)}dA \tag{5}$$

which form the basis of the finite element formulation. The microforce part, Eq. (5) only applies during plastic flow, $\dot\gamma^{(\beta)} > 0$. Corresponding classical balance and microforce balance are:

$$\sigma_{ij,j} = 0 \tag{6}$$

and

$$\pi^{(\beta)} - \tau^{(\beta)} - \xi_{i,i}^{(\beta)} = 0. \tag{7}$$

The stress σ_{ij} is given in the rate form

$$\dot\sigma_{ij} = C_{ijkl}\dot u_{k,l} - C_{ijkl}\sum_\alpha \dot\gamma^{(\alpha)}P_{kl}^{(\alpha)} \tag{8}$$

with $\dot{(\,)} = \partial()/\partial t$, where t is time.

Attention is focused on rate independent material behavior and cases where the GNDs only affect the energetic hardening. Taking

$$\pi^{(\beta)} = \sigma^{(\beta)}\mathrm{sgn}\dot\gamma^{(\beta)} \tag{9}$$

with $\sigma^{(\beta)}$ having the initial value σ_0 for all β and evolving as

$$\dot\sigma^{(\beta)} = \sum_\alpha h^{(\beta\alpha)}|\dot\gamma^{(\alpha)}| \qquad h^{(\alpha\beta)} = qH_0 + (1-q)H_0\delta_{\alpha\beta} \tag{10}$$

where H_0 is the hardening modulus and q is the latent hardening ratio. The relation (9) applies only when there is flow on slip system β, i.e. when $\dot\gamma^{(\beta)} \neq 0$.

The micro-stress $\xi_i^{(\beta)}$ is taken to be given by

$$\xi_i^{(\beta)} = \ell^2\sigma_0 e_{ipq}m_p^{(\beta)}\alpha_{rq}s_r^{(\beta)}, \tag{11}$$

where e_{ipq} is the alternating tensor and α_{ij} is the Nye dislocation density tensor [1]. As here attention is confined to plane strain calculations, $s_3^{(\beta)} = 0$ and $m_3^{(\beta)} = 0$ for all slip systems, the non-vanishing terms of α_{ij} can be defined as [3]:

$$\alpha_{i3} = \sum_\beta s_i^{(\beta)}\gamma_{,j}^{(\beta)}s_j^{(\beta)} \qquad (i = 1, 2). \tag{12}$$

From orthogonality relation $s_i^{(\beta)} m_i^{(\beta)} = 0$, (11) reduces to

$$\xi_i^{(\beta)} = \ell^2 \sigma_0 s_i^{(\beta)} \sum_{\kappa} s_n^{(\beta)} s_n^{(\kappa)} \gamma_{,j}^{(\kappa)} s_j^{(\kappa)}. \tag{13}$$

The response is elastic when

$$|\tau^{(\beta)} + \xi_{i,i}^{(\beta)}| < \sigma^{(\beta)}. \tag{14}$$

In this case, microforce virtual work (5) is satisfied automatically. This assumption introduces numerical problems, as discussed below.

3 NUMERICAL METHOD

In the nonlocal theory used here, the microforce relation is a global relation whereas in the conventional crystal plasticity it is a local relation, which requires using an entirely different numerical approach from that in a local theory. As slips are independent variables of the problem, their values are calculated from the global microforce balance equation (5).

To perform the spatial integration of Eqs. (4) and (5), the same isoparametric finite elements for both equations are used. In each finite element, u_i and $\gamma^{(\alpha)}$ are related to nodal values of displacements U_i and slips $\Gamma^{(\alpha)}$ by

$$u_i = \sum_{K=1}^{N} \Phi^K U_i^K \qquad \gamma^{(\alpha)} = \sum_{K=1}^{N} \Phi^K \Gamma^{(\alpha),K} \quad , \tag{15}$$

where N is the number of nodes per finite element and Φ is the interpolation function. (Uppercase superscripts, with no summation convention, are used to label finite element nodes.)

Eliminating virtual displacements and slips from Eqs. (4) and (5), for a node K of a representative finite element,

$$R_i^K = \int_{B^e} \dot{\sigma_{ij}} \Phi_{,j}^K dV - \int_{\partial B_t^e} \dot{t}_i \Phi^K dA = 0 \tag{16}$$

and

$$r^{K,(\beta)} = \int_{B^e} \left[\left(\dot{\pi}^{(\beta)} - \dot{\tau}^{(\beta)} \right) \Phi^K + \dot{\xi}_i^{(\beta)} \Phi_{,i}^K \right] dV - \int_{\partial B_q^e} \dot{q}^{(\beta)} \Phi^K dA = 0. \tag{17}$$

After assembly, it is obtained the global relations $\mathbf{R} = \mathbf{0}$ and $\mathbf{r} = \mathbf{0}$. An iterative method is used to solve the global equations. The process has two steps that are repeated recursively until convergence. In the first, Eq. (16) is expanded to lowest order considering slips blocked:

$$\mathbf{R}_{(i)} + \left. \frac{\partial \mathbf{R}}{\partial \dot{\mathbf{U}}} \right|_{(i)} (\dot{\mathbf{U}}_{(i+1)} - \dot{\mathbf{U}}_{(i)}) = \mathbf{0}. \tag{18}$$

In the second, Eq. (17) is expanded to lowest order considering displacements blocked:

$$\mathbf{r}_{(i)} + \left. \frac{\partial \mathbf{r}}{\partial \dot{\mathbf{\Gamma}}} \right|_{(i)} (\dot{\mathbf{\Gamma}}_{(i+1)} - \dot{\mathbf{\Gamma}}_{(i)}) = \mathbf{0}. \tag{19}$$

Here, $\dot{\mathbf{U}}$ and $\dot{\mathbf{\Gamma}}$ are the global displacement rate and slip rate vectors, respectively. The subscripts refer to the iteration number. The matrix $\partial \mathbf{R} / \partial \dot{\mathbf{U}}$ is the standard elastic stiffness matrix and $\partial \mathbf{r} / \partial \dot{\mathbf{\Gamma}}$ is the microforce stiffness matrix.

The solution at time t is assumed known. To obtain the solution at time $t + dt$, an increment of loading is prescribed and the values of $\dot{\mathbf{U}}(t)$ and $\dot{\mathbf{\Gamma}}(t)$ are identified with $\dot{\mathbf{U}}_{(i)}$ and $\dot{\mathbf{\Gamma}}_{(i)}$. From the solution to Eqs. (18) and (19), which are a set of linear equations for the rate quantities $\dot{\mathbf{U}}_{(i+1)}$ and $\dot{\mathbf{\Gamma}}_{(i+1)}$, the values of all field quantities at iteration $i + 1$ can be calculated. The value of the L^2 norm of the residuals, $\|\mathbf{R}\|$ and $\|\mathbf{r}\|$ are calculated. If these are greater than a relative tolerance of 10^{-3}, the updated field quantities are used as the new estimate for the state at time $t + dt$ and the process is repeated until the specified tolerance is met.

3.1 Definition of an artificial viscous effect

If a Gauss point is elastic, it will not contribute to integration of Eq. (5). The result is a corresponding micro-stiffness matrix that can be ill-conditioned or singular. In order to avoid this problem, in this work is considered that Eq. (5) is always valid, with a slip resistance $\pi^{(\beta)}$ that follows the definition in (9). $h^{(\beta\alpha)}$ is defined as:

$$h^{(\beta\alpha)} = k\ \delta_{\beta\alpha} \tag{20}$$

and $\sigma_0 = 0$.

The slip rates computed for elastic points are not used to update the stress at these points; the stress update is elastic.

It is worth emphasizing that the method proposed here is basically a mixed method that uses what could be viewed as an artificial viscosity in the microforce virtual work to obtain a unique set of slips. In fact, this mixed formulation can be used for local crystal plasticity as well as for the higher order theory on which attention here is mainly focused.

In the present formulation constitutive equations are only satisfied in average, or when Eq. (5) is satisfied. There is not guarantee that corresponding microforce balance at integration points (Eq. 7) are satisfied exactly. The behavior is problem dependent and also depends on aspects of the numerical procedure such as the equation solver and the numerical precision involved. In order to explore the feasibility of this approach, some simple problems were analyzed for crystals with one, two or three slip systems. When one or two slip systems are activated, Eq. (7) is satisfied using low values of k ($k < H_0$). If three slip systems are activated, the use of such low values of k leads to ill-conditioned stiffness matrices and unstable solutions. If large values of k are used ($k > 10^5 H_0$), solution presents numerical locking and Eq. (7) exhibits a substantial error, even if globally error is acceptable. The effect of locking is more important with three active slip systems but also occurs for one or two active systems. In all cases, the possibility of convergence and the number of iterations to achieve equilibrium depends on the value of k used. While iterations continue until the minimal relative tolerance for $\|\mathbf{R}\|$ and $\|\mathbf{r}\|$ is attained, this level of accuracy is not the same in general when considering Eq. (7).

Eight node isoparametric biquadratic elements with serendipity interpolation functions are used. Within each element integration uses $3x3$ Gauss points. Elements, interpolation functions and integration are the same for slips and displacements. It is possible that, analogous to approaches used for locking due to incompressibility, using different polynomials to interpolate slips and displacements could eliminate locking of slips, but this possibility is not pursued here. Equation system is solved by Gauss elimination direct method [28].

In order to explore the efficacy of this numerical method in a non-trivial context the wedge indentation of single crystals is analyzed.

4 NUMERICAL EXPERIMENTATION

The boundary-value problem of wedge indentation of a single crystal is illustrated in Fig. 1. The depth of indentation is denoted h and the nominal contact area is $a_N = 2h/\tan\phi$, where ϕ is the indenter angle relative to the indented surface. The nominal hardness is $H_N = F/a_N$, where F is the applied force per unit thickness of the indenter. The contact area accounting for pile-up or sink-in is denoted a and is measured from the indenter tip to the furthest point in contact with the indenter (the end-to-end contact area). The "true" hardness is defined as $H = F/a$.

Perfect sticking is assumed between the crystal and the indenter. Symmetry about the indenter tip is assumed so that $u_1 = 0$ on $x_1 = L$ and $u_2 = 0$ on $x_2 = 0$. Attention is confined to small values of the indentation depths h to minimize the effects of external boundaries.

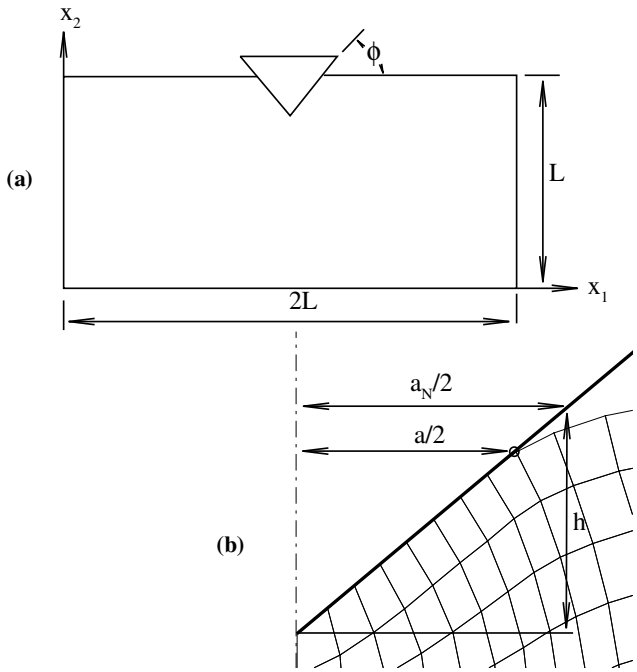

Figure 1: (a) Sketch of the boundary-value problem in the indentation of a single crystal. (b) Detail of the contact zone showing definition of the areas a_N and a.

A 29×29 finite element quadrilateral mesh is used in all the calculations. Slips are concentrated in a refined region of approximately 12×12 elements. These elements present a size ratio that is not larger than 2:1, being the smaller size approximately $L/600$.

Analyses are carried out for two cases. In the first, an indenter with $\phi = 40°$ and a sharp tip is taken into account. In the second, an indenter with $\phi = 45°$ and a rounded tip with a 1 μm radius is used. The two materials defined in Table 1 are considered. All slip systems have the initial strength σ_0. Properties for material 1 and 2 are approximately representative of the aluminum and nickel, respectively.

The numerical parameter k is fixed at $k/H_0 = 10^3$ for all calculations.

Table 1: Material properties (slip system angles are measured relative to the x_1-axis).

material	slip system orientations	G (MPa)	G/H_0	ν	σ_0 (MPa)	q
1	$(60°/120°/0°)$	26120	373	0.34	100	1.4
2	$(54.7°/0°/125.3°)$	76220	254	0.312	175	1.4

4.1 Sharp tip indenter

Different characteristic lengths (ℓ) (see Eq. (11)) are tested in this case. Two higher order boundary conditions are introduced: a condition of the form $\gamma^{(\beta)} = 0$ is referred to as a micro-clamped boundary condition and a condition of the form $q^{(\beta)} = 0$ is termed micro-free.

When the crystal boundary is known a priori, application of the micro-clamped boundary condition is straightforward. In the present case however, boundary with the indenter depends on the contact evolution. The micro-clamped boundary condition must be applied only when contact is detected. A penalty method is used here to impose the micro boundary condition in a similar way the contact condition is imposed [31]. At points of the boundary where contact is detected, $q^{(\beta)}$ assumes the value:

$$q^{(\beta)} = \frac{1}{\chi}\gamma^{(\beta)} \tag{21}$$

where χ is a small positive value. Replacing Eq. (21) into Eq. (17) it can be seen that $q^{(\beta)}$ introduces a contribution $(1/\chi)$ for the microforce stiffness matrix at the corresponding finite element in contact. Then the micro-clamped boundary condition is satisfied as long as χ is close to zero.

Due to the greater hardening induced by nonlocal terms, a greater sink-in of the indenter occurs. This fact is also observed in discrete dislocation calculations in Balint et al. [32]. In fact, the sink-in correction of the area calculation, as shown in Fig. 1, can be inaccurate. Depending on the higher order boundary condition imposed, contact area is not continuous at the indenter-crystal interface, as seen in Fig. 2. In this figure, details of the finite element boundary in the contact area, for two different depths of indentation, are shown. Also two different values of the characteristic length ℓ are considered. In the figure ℓ is parameterized by the characteristic length of the finite element mesh (c). This parameterization is necessary in order to render results mesh independent. Micro-clamped and micro-free boundary conditions are considered. In the first case, when only one node is in contact, the crystal surface tends to deform less around the node, since γ is prescribed to be zero in all slip systems of it, creating a curvature (concave down) around the tip and a gap between indenter and crystal. The phenomenon is restricted to the finite element in contact with the indenter tip. If the characteristic length is increased, the effect tends to be larger, as seen in Fig. 2, however still confined to only one finite element. This observation can be an indication that the effect is, in fact, only a mesh effect. Then a inflection point is observed and a curvature with different sign (concave up) evolve. In the $\ell/c = 24$ case, the inflection point is likely to form again away from the tip (deeper indentation, Fig. 2), changing again the sign of the curvature. Therefore, the area used here to calculate hardness for the micro-clamped boundary condition is actually largely overestimated, especially at shallow indentations. This phenomenon does not occur for micro-free boundary conditions and therefore could not be captured by lower order theories.

In Fig. 3(a),(b) are shown the evolution of H/σ_0 as a function of the relation h/ℓ for micro-clamped and micro-free boundary conditions, respectively. Different values of ℓ are considered, for a fixed mesh spacing c. Local case is also shown in Fig. 3 (in this case, ℓ is chosen an arbitrary value). It is observed that, contrary to the local case and despite some scattering, hardness is basically a function

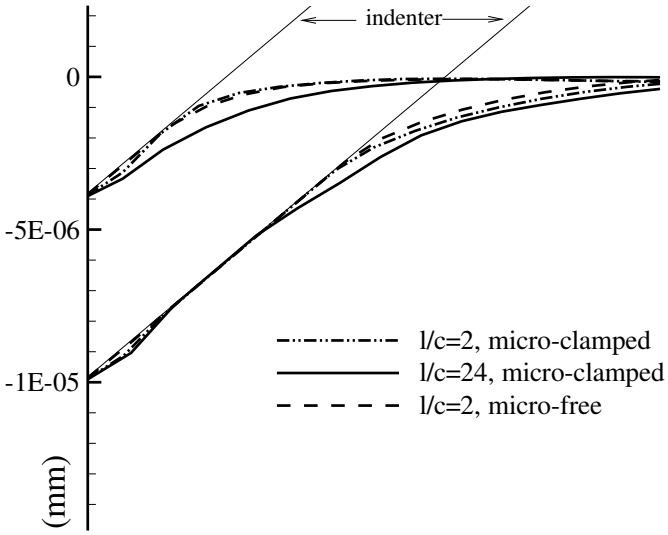

Figure 2: Evolution of the crystal boundary at the contact region, for micro-free boundary condition and micro-clamped boundary condition.

of h/ℓ, the only relevant length scales involved in the model. Qualitatively, the results shown here reproduce the behavior obtained experimentally [33], numerically [34] and also by analytical models [35, 37]. In particular, in the model outlined by Nix and Gao [35], hardness can be estimated as:

$$\frac{H}{H_i} = \sqrt{1 + \frac{h^*}{h}} \tag{22}$$

where H_i and h^* are constants of the model. The first corresponds to the hardness in the limit of infinite depth (local hardness) and the second is a function of the material and indenter angle ϕ. The dependence on the square-root originates from the Taylor hardening assumption made by Nix and Gao [35], where the flow strength is a function of the square-root of the dislocation density. The characteristic length h^* should not be misinterpreted as the characteristic length used in the nonlocal calculations (ℓ), which depends solely on the material. Plots of the Eq. (22) are also included in Fig. 3(a),(b), where h^* is considered as 0.9ℓ (micro-clamped) or 0.7ℓ (micro-free), both obtained by curve fitting with all numerical results.

Finally, it is important to point out that the size effect observed in indentation is directly linked to the density of GNDs and can be captured regardless the presence of higher order terms, as shown by Nix and Gao [35]. For instance, the effect is captured by Lee and Chen [36], where a lower order theory is applied to the indentation of a single crystal with multiple active slip systems. However, higher order terms can lead to different distributions of the density of GNDs, as discussed below. In addition, the consideration of these terms can change the behavior on the unloading of the indenter, when compared to lower order theories, but this aspect is not explored in the present work.

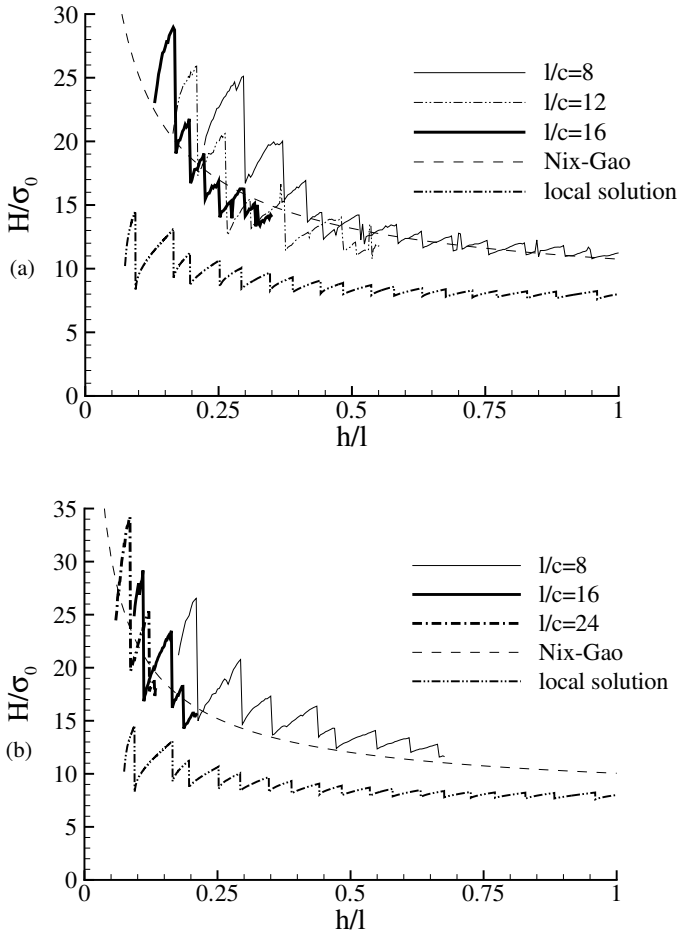

Figure 3: Hardness (H/σ_0) as a function of the ratio (h/ℓ) for different length scales (ℓ) considering (a) micro-clamped boundary condition and (b) micro-free boundary condition. Analytical solution by Nix and Gao [35] and local solution are also included. Material 1.

4.2 Rounded tip indenter

In order to investigate further the effect of higher order boundary conditions, an analysis modeling the situation experimentally studied by Kysar et al. [30] is carried out. In this case, indenter has an angle $\alpha = 45^\circ$ with a round tip with radius $r = 1\mu$m. Material 2 (Table 1) is used in the calculations.

In this example, Kysar et al. [30] calculate the Nye dislocation density tensor α_{ij} based on experimentally measured crystal rotations. The method is based on the relation of α_{ij} with the crystal lattice curvature tensor κ_{ji} [38], defined as $\kappa_{ji} = \partial\omega_j/\partial x_i$, where ω_j is the lattice rotations about $j-$axis. In the plane case considered, neglecting gradients of elastic strains, the non-vanishing terms of the Nye tensor are $\alpha_{i3} = -\kappa_{3i}$, with $i = 1, 2$. Considering the component α_{13}, Kysar et al. [30] show that the largest magnitude of α_{13} occurs at the symmetry line, where the lattice rotation has an abrupt change in sign. This effect is also predicted by continuum crystal plasticity in Bouvier and Needleman [29] and by the discrete dislocation calculations in Balint et al. [32]. The result is a zone in which α_{13} is predominantly positive (negative curvature of the lattice). This region is flanked by

negative values of α_{13} which in turn are flanked by positive values, further away from the symmetry line. These changes in sign are related to inflection points in the lattice curvature.

Figure 4 shows the computed distribution of α_{13} of the Nye tensor calculated from Eq. (12) for the two higher order boundary conditions considered ($\ell/c = 3.7$ and $k/H_0 = 5x10^3$). Figure 4(a) shows the distribution for the micro-free boundary condition and Fig. 4(b) shows the distribution for the micro-clamped boundary condition. Neither of these boundary conditions reproduce the activity at the symmetry line found by Kysar et al. [30]. This may be a consequence of neglecting crystal rotation effects. Nevertheless, the calculations with both higher order boundary conditions are able to qualitatively reproduce the development of the other regions. In the case of the micro-clamped boundary condition at the indenter-crystal interface, however, a zone with strong positive values of α_{13} is seen in most of the contact region. One possible explanation is the warp created by the micro-clamped boundary condition at the contact interface, as seen in Fig. 2. This behavior is in disagreement with the observations by Kysar et al. [30] and is not a trend observed in the case of micro-free boundary condition either.

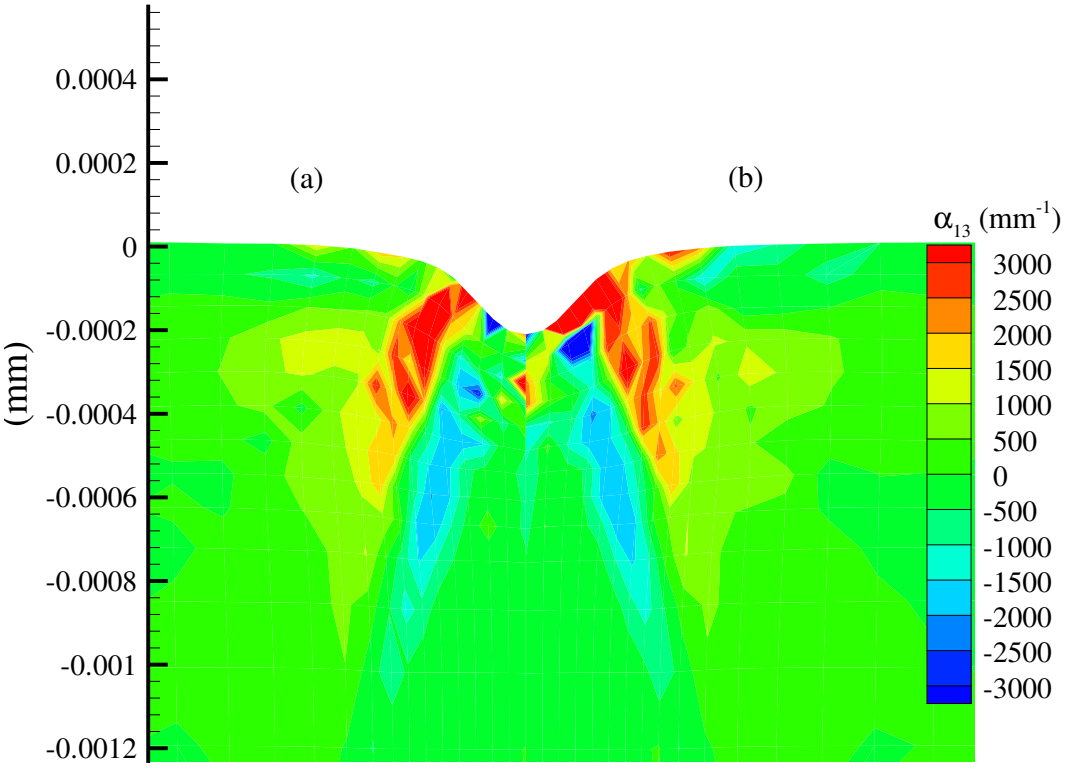

Figure 4: Contours of the Nye tensor component α_{13} for two different high order boundary conditions: Micro-free (a) and micro-clamped (b). Material 2.

In the plain strain cases considered, the Nye tensor is equal to the net Burgers vector per unit area [3] and can be a associated to the density of GNDs. Fig. 5 shows contours of the L^2 norm of α_{i3},

with $i = 1, 2$. While the distribution of GNDs in the micro-free boundary condition case, Fig. 5(a), is diffused below contact area without any discerning pattern, in the micro-clamped boundary condition case, Fig. 5 (b), a zone of intense development of GNDs near the contact zone is seen. The latter case presents a behavior inconsistent with results obtained by Kysar et al. [30] which suggests that the micro-clamped boundary condition may not be an appropriate higher order boundary condition for indentation.

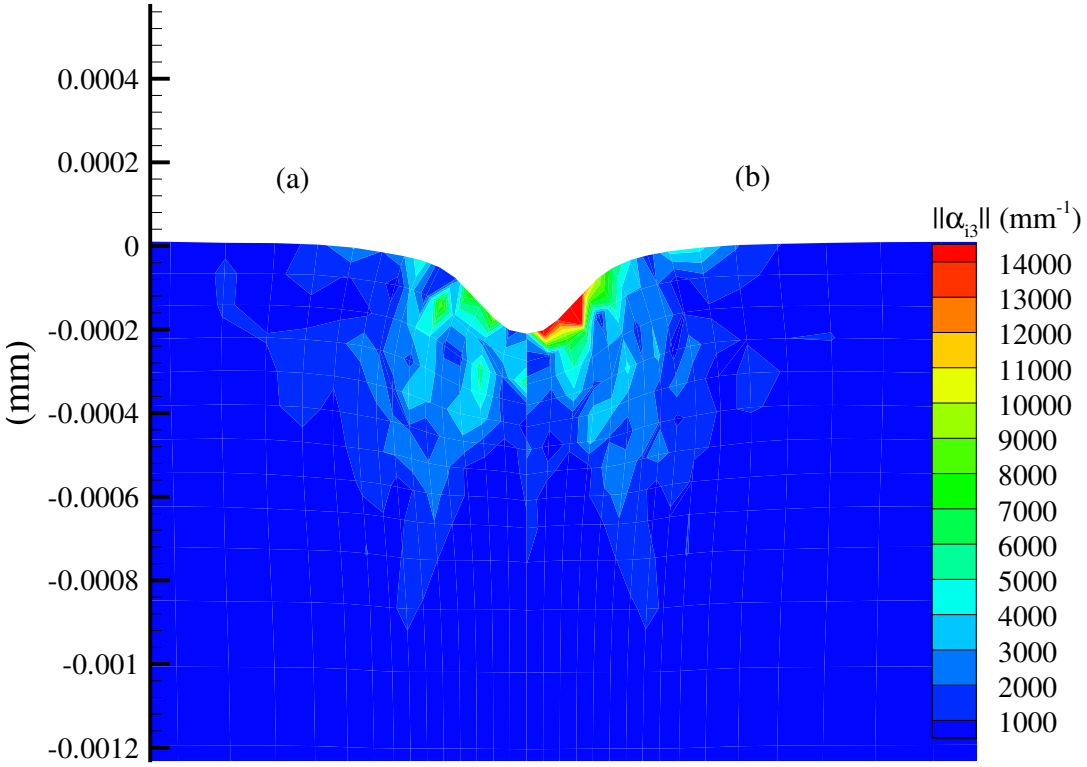

Figure 5: Contours of the Norm of the Nye tensor α_{i3}, where $i = 1, 2$, for two different high order boundary conditions: Micro-free (a) and micro-clamped (b). Material 2.

5 CONCLUDING REMARKS

The approach proposed here considers, as for the rate dependent cases, all points contributing to the microforce balance and, as for the rate independent case, slips in the constitutive relation only for elastic points. A numerical parameter k is introduced to restrict or penalize slips at elastic points. Regarding numerical behavior of the algorithm, the following conclusions can be made:

- The value of k is important on the solution when the elastic and plastic behavior are occurring concomitantly in the domain.

- For k tending to zero, the developed model tends to behave as a pure rate independent solution. Stiffness matrices in this case tend to be non-positive definite.

- If the behavior is totally plastic, the discussion about k becomes irrelevant. Depending on crystal properties and deformation gradient imposed by boundary conditions, solution may be impossible or unstable, at least for the system solver used in this study.

Despite these numerical difficulties, it was possible to solve wedge indentation problems. Comparisons with other models and with measured data, when possible, presented a good match. Considering the influence of higher order terms, it is concluded that:

- It was possible to capture size effects in the indentation problem considering a situation where GNDs only affect kinematic hardening. Behavior obtained follows the model developed by Nix and Gao [35].

- Results suggest that micro-free boundary conditions are more suitable than micro-clamped higher order boundary conditions to model the indenter-crystal interface, when comparing distribution of GNDs [30]. This is only a preliminary conclusion based on the simplified model used in this study, where slip rotations are not considered.

ACKNOWLEDGMENTS

The author is pleased to acknowledge support from the Brazilian Government through a CNPq Fellowship. Also, the author would like to thank Prof. A. Needleman of the University of North Texas for his discussions on the subject.

REFERENCES

[1] J.F. Nye, (1953), "Some geometrical relations in dislocated solids", Acta Metall. 1 153–162.

[2] M.F. Ashby, (1970),"The deformation of plastically non-homogeneous materials", Philos. Mag. 21 399–424.

[3] N.A. Fleck, G.M. Muller, F. Ashby, J.W. Hutchinson, (1994), "Strain gradient plasticity: theory and experiment", Acta Metall. Mater. 42 475–487.

[4] Q. Ma, D.R. Clark, (1995), "Size dependent hardness of silver single crystals", J. Mater. Res. 10 853–863.

[5] J.S. Stolken, A.G. Evans, (1998), "A microbend test method for measuring the plasticity length scale", Acta Mater. 46 5109–5115.

[6] J.Y. Shu, N.A. Fleck, (1999), "Strain gradient crystal plasticity: size-dependent deformation of bicrystals", J. Mech. Phys. Solids 47 297–324.

[7] M.E. Gurtin, (2002), "A gradient theory of single-crystal viscoplasticity that accounts for geometrically necessary dislocations", J. Mech. Phys. Solids 50 5–32.

[8] M.E. Gurtin, (2008), "A finite-deformation, gradient theory of single-crystal plasticity with free energy dependent on densities of geometrically necessary dislocations", Int. J. Plasticity 24 702–725.

[9] A. Arsenlis, D.M. Parks, R. Becker, V.V. Bulatov, (2004), "On the evolution of crystallographic dislocation density in non-homogeneously deforming crystals", J. Mech. Phys. Solids 52 1213–1246.

[10] L.P. Evers, W.A.M. Brekelmans, M.G.D. Geers, (2004), "Non-local crystal plasticity model with intrinsic SSD and GND effects" J. Mech. Phys. Solids 52 2379–2401.

[11] J.R. Mayeur, D.L. McDowell, D.J. Bammann, (2011), "Dislocation-based micropolar single crystal plasticity: comparison of multi and single criterion theories" J. Mech. Phys. Solids 59 398-422.

[12] A. Acharya, J.L. Bassani, (2000), "Incompatibility and crystal plasticity", J. Mech. Phys. Solids 48 1565–1595.

[13] A. Acharya, A.J. Beaudoin, (2000), "Grain size effects in viscoplastic polycrysals at moderate strains", J. Mech. Phys. Solids 48 2213–2230.

[14] C.S. Han, H.J. Gao, Y.G. Huang, W.D. Nix, (2005), "Mechanism-based strain gradient crystal plasticity - I. Theory", J. Mech. Phys. Solids 53 1188–1203.

[15] J.Y. Shu, N.A. Fleck, E. Van der Giessen, A. Needleman, (2001), "Boundary layers in constrained plastic flow: comparison of nonlocal and discrete dislocation plasticity", J. Mech. Phys. Solids 49 1361–1395.

[16] E. Bittencourt, A. Needleman, M.E. Gurtin, E. Van der Giessen, (2003), "A comparison of nonlocal continuum and discrete dislocation plasticity predictions", J. Mech. Phys. Solids 51 281–310.

[17] L. Anand, M.E. Gurtin, S.P. Lele, C. Gething, (2005), "A one-diemensional theory of strain-gradient plasticity: formulation, analysis, numerical results", J. Mech. Phys. Solids 53 1789–1826.

[18] D. Okumura, Y. Higashi, K. Sumida, N. Ohno, (2007), "A homogenization theory of strain gradient single crystal plasticity and its finite element discretization" Int. J. Plasticity 23 1148–1166.

[19] J.M. Gerken, P.R. Dawson, (2008), "A finite element formulation to solve a non-local constitutive model with stresses and strains due to slip gradients", Comp. Meth. Appl. Mech. Eng. 197 1343–1361.

[20] M. Kuroda, (2011), "On large-strain finite element solutions of higher-order gradient crystal plasticity", Int. J. Solids Struct. 48 3382-3394.

[21] R. Hill, J.R. Rice, (1972), "Constitutive analysis of elasto-plastic crystals at arbitrary strain", J. Mech. Phys. Solids 20 401–413.

[22] D. Peirce, R.J. Asaro, A. Needleman, (1982), "An Analysis of nonuniform and localized deformation in ductile single-crystals", Acta metall. 30 1087–1119.

[23] D. Peirce, R.J. Asaro, A. Needleman, (1983), "Material rate dependence and localized deformation in crystalline solids", Acta metall. 31 1951–1976.

[24] A.R. Zamiri, F. Pourboghrat, (2010), "A novel yield function for single crystal based on combined constraints optimization", Int. J. Plasticity 26 731–746.

[25] L. Zhang, R. Dingreville, T. Bartel, M.T. Lusk, (2011), "A stochastic approach to capture crystal plasticity", Int. J. Plasticity 27 1432–1444.

[26] E. Bittencourt, A. Needleman, Rate-dependent nonlocal crystal plasticity: implementation and boundary layers, in: A. Cardona, M. Storti, C. Zuppa (Eds.), Mecanica Computacional, AMCA, San Luis, 2008, pp. 1177–1192.

[27] U. Borg, C.F. Niordson, N.A. Fleck, V. Tvergaard, (2006), "A viscoplastic strain gradient analysis of materials with voids or inclusions", Int. J. Solids Struct. 43 4906–4916.

[28] K.-J. Bathe, Finite Element Procedures in Engineering Analysis. Prentice Hall, Englewood Cliffs, 1982.

[29] S. Bouvier, A. Needleman, (2006), "Effect of the number and orientation of active slip systems on plane strain single crystal indentation", Model. Simul. Mat. Sci. Engin. 14 1105–1125.

[30] J.W. Kysar, Y. Saito, M.S. Oztop, D. Lee, W.T. Huh, (2010), "Experimental lower bounds on geometrically necessary dislocation density" Int. J. Plasticity 26 1097-1123.

[31] E. Bittencourt, G.J. Creus, (1998), "Finite element analysis of three-dimensional contact and impact in large deformation problems", Comput. Struct. 69 219–234.

[32] D.S. Balint, V.S. Deshpande, A. Needleman, E. Van der Giessen, (2006), "Discrete dislocation plasticity analysis of the wedge indentation of films", J. Mech. Phys. Solids 54 2281–2303.

[33] J. Lou, P. Shrotriya, T. Buchheit, D. Yang, W.O. Soboyejo, (2003), "Nanoindentation study of plasticity length scale effects in LIGA Ni microelectromechanical systems structures", J. Mater. Res. 18 719–728.

[34] A. Widjaja, A. Needleman, E. Van der Giessen, (2007), "The effect of indenter shape on submicron indentation according to discrete dislocation plasticity", Modell. Simul. Mat. Sci. Engin. 15 S121–S131.

[35] W.D. Nix, H. Gao, (1998), "Indentation size effects in crystalline materials: A law for strain gradient plasticity", J. Mech. Phys. Solids 46 411–425.

[36] W.B. Lee, Y.P. Chen, (2010), "Simulation of micro-indentation hardness of FCC single crystals by mechanism-based strain gradient crystal plasticity", Int. J. Plasticity 26 1527–1540.

[37] Z. Xue, Y. Huang, K.C. Hwang, M. Li, (2002), "The influence of indenter tip radius on the micro-indentation hardness", J. Eng. Mater. T. ASME 124 371–379.

[38] A. Arsenlis, D.M. Parks, (1999), "Crystallographic aspects of geometrically-necessary and statistically-stored dislocation density", Acta Mater. 47 1597–1611.

[39] R. De Borst, H.-B. Mülhaus, (1992), "Gradient-dependent plasticity: formulation and algorithmic aspects", Int. J. Numer. Methods Eng. 35 613–618.

[40] S.P. Lele, L. Anand, (2008), "A small-deformation strain-gradient theory for isotropic viscoplastic materials", Phil. Mag. 88 3655–3689.